Fibroblast growth factor 21 is induced upon cardiac stress and alters cardiac lipid homeostasis

Manoja K. Brahma,[1,*] Rene C. Adam,[1,*] Nina M. Pollak,[*] Doris Jaeger,[*] Kathrin A. Zierler,[*] Nadja Pöcher,[*] Renate Schreiber,[*] Matthias Romauch,[*] Tarek Moustafa,[*] Sandra Eder,[*] Thomas Ruelicke,[†,§] Karina Preiss-Landl,[*] Achim Lass,[*] Rudolf Zechner,[*] and Guenter Haemmerle[2,*]

Institute of Molecular Biosciences,* University of Graz, 8010 Graz, Austria; Biomodels Austria† and Institute of Laboratory Animal Science,§ University of Veterinary Medicine, 1210 Vienna, Austria

Abstract **Fibroblast growth factor 21 (FGF21) is a PPARα-regulated gene elucidated in the liver of PPARα-deficient mice or PPARα agonist-treated mice. Mice globally lacking adipose triglyceride lipase (ATGL) exhibit a marked defect in TG catabolism associated with impaired PPARα-activated gene expression in the heart and liver, including a drastic reduction in hepatic FGF21 mRNA expression. Here we show that FGF21 mRNA expression is markedly increased in the heart of ATGL-deficient mice accompanied by elevated expression of endoplasmic reticulum (ER) stress markers, which can be reversed by reconstitution of ATGL expression in cardiac muscle. In line with this assumption, the induction of ER stress increases FGF21 mRNA expression in H9C2 cardiomyotubes. Cardiac FGF21 expression was also induced upon fasting of healthy mice, implicating a role of FGF21 in cardiac energy metabolism. To address this question, we generated and characterized mice with cardiac-specific overexpression of FGF21 (CM-Fgf21). FGF21 was efficiently secreted from cardiomyocytes of CM-Fgf21 mice, which moderately affected cardiac TG homeostasis, indicating a role for FGF21 in cardiac energy metabolism. Together, our results show that FGF21 expression is activated upon cardiac ER stress linked to defective lipolysis and that a persistent increase in circulating FGF21 levels interferes with cardiac and whole body energy homeostasis.**—Brahma, M. K., R. C. Adam, N. M. Pollak, D. Jaeger, K. A. Zierler, N. Pöcher, R. Schreiber, M. Romauch, T. Moustafa, S. Eder, T. Ruelicke, K. Preiss-Landl, A. Lass, R. Zechner, and G. Haemmerle. **Fibroblast growth factor 21 is induced upon cardiac stress and alters cardiac lipid homeostasis.** ***J. Lipid Res.*** **2014.** 55: **2229–2241.**

Supplementary key words adipose triglyceride lipase • cardiac lipid and energy metabolism • ER stress

Fibroblast growth factor 21 (FGF21) is an important regulator in energy metabolism, and the hormone-like properties of FGF21 are implicated in the adaptation to energy restriction and fasting (1–3). FGF21 is most abundantly expressed in the liver of fasted mice and is released into the circulation, where the protein shows pleiotropic effects on target tissues including adipose tissue, pancreatic islets, and the liver itself (4–6). The action of FGF21 in the periphery and in the liver is mediated via binding to FGF receptors in a β-Klotho-dependent manner (7–9). FGF21 mRNA expression is largely controlled by PPARα, a nuclear receptor that induces the expression of numerous genes implicated in mitochondrial FA uptake and mitochondrial FA oxidation (FAO) (10).

During food restriction, the catabolism of TGs and the generation of FAs are important energy sources, and FAs that are used for mitochondrial β oxidation can originate from exogenous sources (i.e., from adipose tissue TG mobilization or from endogenous TG catabolism of intracellular TG depots) (11). In most if not all organs, the first and rate-limiting step in TG catabolism is catalyzed by adipose triglyceride lipase (ATGL), which generates diglycerides (12, 13). Efficient ATGL-mediated TG catabolism depends on the presence of the ATGL coactivator protein comparative gene identification-58 (CGI-58) (14). Mice lacking CGI-58 in muscle exhibit severe cardiac steatosis linked to impaired PPARα-target gene expression (15). More recently, we and others demonstrated that ATGL-mediated TG catabolism is tightly coupled to PPARα-induced gene expression and accordingly to the induction of mitochondrial FAO (16–18). The interconnection of lipolysis, PPARα-activated gene expression, and mitochondrial FAO is most exemplified in mice lacking ATGL:

This work was supported by the Austrian Ministry for Science and Research and the grants Fonds zur Förderung der wissenschaftlichen Forschung (FWF) project DK-MCD W1226, P20602-B05 and SFB LIPOTOX F30-B05, which are funded by the Austrian Science Fund.

Manuscript received 9 October 2013 and in revised form 14 August 2014.

Published, JLR Papers in Press, August 31, 2014
DOI 10.1194/jlr.M044784

Abbreviations: ATGL, adipose triglyceride lipase; CGI-58, comparative gene indentification-58; CM, cardiac muscle; 2-DG, 2-deoxy-D-glucose; ER, endoplasmic reticulum; FAO, fatty acid oxidation; FGF21, fibroblast growth factor 21; LacZ, β-galactosidase; MHX, myosin heavy chain; MOI, multiplicity of infection; RQ, respiratory quotient.

[1] Manoja K. Brahma and Rene C. Adam contributed equally to this work.
[2] To whom correspondence should be addressed.
e-mail: guenter.haemmerle@uni-graz.at

defective TG catabolism in ATGL-deficient mice provokes severe cardiac steatosis and increased hepatic TG levels due to a defect in PPARα-activated gene expression and FAO in the heart and liver, respectively (16, 17). In accordance with this defect, hepatic FGF21 mRNA expression levels are drastically reduced in ATGL-deficient mice, leading to a marked drop in circulating FGF21 protein levels (19). Here we show that FGF21 mRNA expression is substantially increased in cardiac muscle (CM) of mice globally lacking ATGL or specifically lacking the ATGL coactivator comparative gene identification-58 (CGI-58) in muscle despite reduced mRNA expression of established PPARα-regulated and coregulated genes. Increased cardiac FGF21 mRNA expression was paralleled by cardiac ER stress observed in CM of ATGL-deficient mice. The similar induction of FGF21 expression in H9C2 cardiomyotubes when exposed to ER stress may suggest that FGF21 expression is triggered by cardiac ER stress. Yet, the induction of FGF21 mRNA expression in CM of fasted WT mice together with changes in cardiac TG homeostasis of mice with cardiac-specific FGF21 overexpression may suggest a physiological role of FGF21 in cardiac energy metabolism.

MATERIALS AND METHODS

Animals

Mice globally lacking ATGL were generated as previously described (12). Mice expressing ATGL solely in CM were generated by breeding the ATGL transgene onto an ATGL-deficient background (16). Mice with muscle-specific CGI-58 disruption and transgenic mice overexpressing *Perlipin 5* in the heart were generated as previously described (15, 20). The PPARα agonist Wy14,643 (Cayman Chemical Co., Ann Arbor, MI) was provided via ad libitum feeding a chow diet containing 0.1% Wy14,643 for 2 weeks. Transgenic mice expressing mouse *Fgf21* cDNA under the control of the cardiomyocyte-specific α-myosin heavy chain (α-MHC) promoter (*Myh6*, Genbank: accession number U71441) were generated by cloning mouse *Fgf21* cDNA (amplified from a liver cDNA using the 5′-GA GTC GAC ATG GAA TGG ATG AGA TCT AGA GTT G-3′ forward and 5′-AG GTC GAC AGA GTC AGG ACG CAT AGC TTG -3′ reverse primers including a *Sal*I restriction site at the 5′ sites, which are underlined and used for cloning) in the α-MHC promoter construct (21), kindly provided by J. Robbins. Characterized transgenic mice originate from a B6D2F2 background and were backcrossed for 3–4 generations on C57BL6 background. Littermates were used for characterization, and mice with cardiac-specific *Fgf21* overexpression (CM-Fgf21) were heterozygous with respect to the integrated transgene. Animals were housed in a specific pathogen-free facility and maintained on a regular light-dark cycle (14 h light, 10 h dark) with ad libitum access to a standard laboratory chow diet (4.5% wt/wt fat; ssniff Spezialdiäten, Germany) and water. For tissue collection, mice were euthanized by cervical dislocation, and excised tissues were immediately snap-frozen. The maintenance, handling, and tissue collection from mice was approved by the Austrian Federal Ministry for Science and Research and by the ethics committee of the University of Graz.

Plasma parameters

Blood samples were collected by retro-orbital puncture from isoflurane-anesthetized mice. Plasma parameters were analyzed by commercially available kits from Wako, Sigma, and Thermo Fisher Scientific, and plasma glucose levels were determined using the FreeStyle Freedom Lite® Blood Glucose Monitoring System (Abbott). Plasma levels of FGF21 and IGF-1 were measured using commercially available ELISAs from Millipore-Merck (USA) and Abnova (Taiwan), respectively.

Measurement of mRNA expression levels by quantitative RT-PCR

Total RNA was extracted with the TRIzol reagent (Invitrogen) and treated with DNaseI (Invitrogen). For first-strand cDNA synthesis, 1 μg of total RNA was reverse transcribed at 37°C for 1 h using random hexamer primer (Applied Biosystems) and Superscript II reverse transcriptase (Invitrogen). Quantitative RT-PCR reactions (20 μl) contained 8 ng of cDNA, 10 pM of each primer, and 10 μl of SYBR Green master mix (Fermentas) and were carried out using ABI-StepOnePlus™ detection system (Applied Biosystems). Relative mRNA levels were quantified using the comparative ΔΔCT method with β-actin as reference gene. Primer sequences are described in detail in the supplementary material.

H9C2 myoblast cell culture and infection with recombinant adenovirus

Rat heart H9C2 myoblast cells were obtained from ATCC and cultured in DMEM containing 4.5 g/l glucose and 10% FCS (Gibco-Invitrogen). H9C2 cells were differentiated by reducing the amount of FCS to 1%. Linear adenoviral DNA, including the coding sequence of murine FGF21 (kindly provided from Steven Kliewer, UT Southwestern Medical School) or β-galactosidase (LacZ), was transfected into HEK293 cells, and large-scale production of high titer recombinant adenovirus was performed according to a standard protocol (22). H9C2 cells were seeded into 6-well culture plates at a density of 200,00 cells/well. After differentiation for 10 days, H9C2 cardiomyotubes were infected with adenovirus encoding for either LacZ or FGF21 at a multiplicity of infection (MOI) of 500 or 750. Unless otherwise indicated, 500 MOI was applied.

Examination of TG homeostasis in H9C2 cardiomyotubes

H9C2 cells were differentiated in 6-well culture dishes and infected with adenovirus encoding either FGF21 or lacZ. Thirty-six hours after infection with recombinant adenovirus, cells were washed twice with PBS and loaded with differentiation medium containing 400 μM oleic acid (complexed with BSA) and 0.4 μCi [^{14}C]oleic acid per well. The next day, incorporation of [^{14}C] oleic acid into the TG moiety was analyzed under basal (presence of differentiation medium) or serum-starved (absence of FCS for 3 h) conditions. Subsequently, cells were washed twice with ice-cold PBS, and lipids were extracted with 2 ml of n-hexane/isopropyl alcohol (3:2, v/v). Extracted lipid samples were separated by TLC using hexane/diethyl ether/acetic acid (70:29:1, v/v/v) as solvent system. TLC bands corresponding to TG were cut and suspended in scintillation cocktail, and radioactivity was determined by liquid scintillation counting (Beckman LS 6500). Cells were lysed with 1 ml of lysis buffer (0.1% SDS and 0.3 N NaOH) for protein quantitation using the bicinchoninic acid assay.

Tissue TG measurement

Tissue lipids were extracted according to the method of Folch (23). Tissue lipids were dried in a stream of nitrogen and redissolved by brief sonication in 2% Triton X-100. TG concentrations

were measured using Infinity Triglycerides Reagent (Thermo Electron Corp., Victoria, Australia).

Glucose uptake in differentiated H9C2 cells

Differentiation of H9C2 cells and infection with recombinant adenovirus was performed as described above. Forty-eight hours after adenovirus infection, the media was replaced by 1 ml of depletion medium (40 mM NaCl, 1.2 mM $MgSO_4$, 1.2 mM KH_2PO_4, 4.7 mM KCl, 0.25 M $CaCl_2$, 2% fatty acid-free BSA) and incubated for 1 h at 37°C. Subsequently, 1 ml of depletion medium and medium containing insulin (100 or 200 nM) was added and incubated for another 15 min. The assay was started by replacing media with transport solution (40 mM NaCl, 1.2 mM $MgSO_4$, 1.2 mM KH_2PO_4, 4.7 mM KCl, 0.25 M $CaCl_2$) containing 5 mM of 2-deoxyglucose and [^{3}H]2-deoxyglucose (0.5 μCi/well). After 5 min incubation, the reaction was stopped by aspirating the transport solution and washing four times with ice-cold PBS (1 ml/well). Cells were lysed with 1 ml of lysis buffer (0.1% SDS and 0.3 N NaOH) for 2 h. For determination of protein concentration, 100 μl of lysate was used, and 800 μl were measured by liquid scintillation counting.

Determination of glucose oxidation in H9C2 cardiomyotubes

Cells were seeded at a density of 6×10^5 in 25 cm^2 culture flasks. After adenovirus infection as described, cells were thoroughly washed and serum starved for 4 h by incubating them in low-glucose DMEM (1g/l) without serum. After serum starvation, cells were incubated with 0.3 μCi/flask of [U-^{14}C]D-glucose (American Radiolabeled Chemicals) for 2 h. NaOH (5 N; 250 μl) was added to a microcentrifuge tube (1.5 ml capacity) and fit into the mouth of the culture flask. The reaction was stopped by the addition of perchloric acid (70%) through the space between the microcentrifuge tube and flask. The flask was tightly closed and wrapped with parafilm. Released $^{14}CO_2$ was trapped for 12 h at 37°C, and thereafter the NaOH solution was transferred to a scintillation vial for radioactivity counting. Then the media in the flasks was aspirated, and cells were lysed with 2 ml of lysis buffer for 2 h before determination of protein content using the BCA assay.

Glucose tolerance test

Mice were fasted for 6 h and then injected intraperitoneally with 1.5 g glucose per kg of body weight. Glucose levels were monitored before and 15, 30, 60, and 120 min after injection using an AccuCheck Glucometer (Roche Diagnostics, Vienna, Austria).

Examination of tissue glucose uptake

Tissue-specific glucose uptake was determined using [^{3}H]2-deoxyglucose (^{3}H-DG). A detailed description of the protocol can be found in the supplementary material.

Determination of cellular FA uptake

FA uptake in differentiated H9C2 cells infected with recombinant LacZ or FGF21 adenovirus was determined by loading cells with 400 μM oleic acid (complexed with BSA) together with 0.4 μCi [^{14}C]oleic acid per well. After incubation for 1 min, cells were washed four times with ice-cold BSA, and 1 ml of 0.3 M NaOH/0.1% SDS was added per well for cell lysis. An aliquot of 20 μl was used for protein measurement, and 750 μl were used for liquid scintillation counting.

Measurement of oleic acid oxidation

FAO in CM homogenates was examined according to the protocol of Hirschey et al. (24) and is described in detail in the supplementary material.

TG hydrolase assay

TG hydrolase assays were performed as previously described (14). A description of the preparation of tissue lysates and detailed assay procedures can be found in the supplementary material.

Induction of ER stress in H9C2 cardiomyotubes

After differentiation, H9C2 cardiomyotubes were incubated with differentiation medium (DMEM with 1% FCS) containing 1 mM of DTT (Sigma Chemical Co., St. Louis, MO) for 4 h at 37°C. After incubation, cells were washed with PBS, and RNA was isolated using 1.8 ml of TRIzol reagent (Invitrogen, Carlsbad, CA). In another approach, differentiated cardiomyotubes were incubated for 24 h in differentiation media containing 200 μM palmitate (complexed with BSA) or tunicamycin (10 μg/ml). DMSO (0.5%) was used as solvent control for treatments with tunicamycin. After incubation, cells were washed with PBS and RNA was prepared as described above.

Western blot analysis

Cardiac tissue of nonfasted mice was homogenized in buffer A (0.25 M sucrose, 1 mM EDTA, 1 mM dithiothreitol, 20 μg/ml leupetine, 2 μg/ml antipain, and 1 μg/ml pepstatin [pH 7.0]) on ice using an Ultra Turrax (Ika GmbH, Staufen, Germany). The homogenate was centrifuged at 20,000 *g* at 4°C for 30 min, and the infranatants were collected and used for Western blot analysis. Proteins were separated by 10% SDS-PAGE followed by Western blot analysis using PVDF membranes (Carl Roth GmbH, Karlsruhe, Germany) and CAPS buffer (10 mM 3-cyclohexylamino-1-propanesulfonic acid, 10% methanol) for protein transfer. Blots were probed using a FGF21 primary antibody (Goat Polyclonal IgG, Sc-16842; Santa Cruz), rabbit monoclonal antibodies for BiP (Grp78) and PDI, goat polyclonal antibody against mouse β-Klotho (R&D Systems), or a GAPDH-specific antibody (Cell Signaling, Boston, MA). For analysis of AMPKα and phosphorylated AMPKα (Thr172), rabbit monoclonal antibodies were applied (Cell Signaling). Specifically, bound immunoglobulins were detected in a second reaction using HRP-conjugated anti-rabbit antibody and visualized by enhanced chemiluminescence detection (GE Healthcare).

For determination of FGF21 released from FGF21 adenovirus-infected cells, 500 μl of TCA (50%) was added to 2 ml of collected medium, mixed uniformly, and put on ice for 1 h. After incubation, media was centrifuged at 16,000 rpm at 4°C for 15 min. The supernatant was discarded, and 1 ml of acetone (80%, v/v) was added to each sample, and samples were again centrifuged at 16,000 rpm at 4°C for 15 min to remove TCA from the pellet. Pellets were resuspended in 50 μl of SDS buffer and loaded onto a SDS protein gel.

Body mass analysis

Body fat and lean mass were determined by a calibrated mini-Spec® NMR analyzer (Bruker Optics, Billerica, MA).

Metabolic cages

Mice were housed in a laboratory animal monitoring system (LabMaster, TSE Systems GmbH, Bad Homburg, Germany) that allows the continuous measurement of oxygen consumption and carbon dioxide elimination of the body for calculating respiratory quotient (RQ, the ratio of carbon dioxide elimination versus oxygen consumption). Mice were allowed to acclimatize for at least 1 day before monitoring parameters and food intake.

Mouse echocardiography

Echocardiographic analyses (25) were performed under light isoflurane anesthesia. A detailed description of the protocol can be found in the supplementary material.

Analysis of cellular respiration

High-resolution respiration analyses were performed in intact, differentiated H9C2 cells at 37°C using Oroboros® Oxygraph O2k (Oroboros Instruments, Innsbruck, Austria). After trypsinization, 1×10^6 H9C2 cells were resuspended in normal growth media, and routine measurements (routine) were performed over 10–15 min until steady-state was reached. Then, 2.5 μM oligomycin was added to inhibit ATP synthase (leak). The chemical uncoupler FCCP was then titrated until maximal respiration (electron transfer system) was obtained. Subsequently, complex I-driven respiration was analyzed upon addition of 1 μM rotenone.

Statistical analysis

Data are presented as mean + SD. Statistical significance was determined by the Student's unpaired two-tailed *t*-test. Group differences were considered significant for $P < 0.05$, $P < 0.01$, and $P < 0.001$.

RESULTS

ER stress in CM of ATGL-deficient mice and induction of ER stress in H9C2 cardiomyotubes are coupled to substantially increased FGF21 expression

Mice globally lacking ATGL (ATGL-ko) show a marked defect in PPARα-activated gene expression in CM and liver (16). In accordance with the established role of FGF21 as a PPARα-regulated gene (1, 3), Jha and colleagues (19) very recently showed a strong reduction in FGF21 mRNA expression in the liver of ATGL-ko mice accompanied by a substantial decrease in circulating FGF21 levels. Here we show that FGF21 mRNA expression is strongly increased (by 11-fold) in CM of ATGL-ko mice (**Fig. 1A**) despite impaired expression of established PPARα-regulated genes (16). The induction of FGF21 expression in CM of ATGL-ko mice could be an adaptation to the strong reduction in hepatic FGF21 mRNA expression and consequently to the decreased circulating FGF21 levels (19). To address this hypothesis, we measured FGF21 mRNA expression in mice expressing ATGL exclusively in CM on an otherwise ATGL-deficient background (ATGL-koTgA). The rescue of ATGL expression solely in CM markedly reduced FGF21 mRNA levels (−67%) in cardiac tissue of fasted mice (Fig. 1A), indicating that the increase in FGF21 mRNA expression of ATGL-ko mice primarily originates from the absence of ATGL in CM. In accordance with this assumption, we found a marked 9.3-fold increase in FGF21 mRNA expression levels in CM of mice lacking the ATGL coactivator CGI-58 exclusively in muscle (supplementary Fig. IA), whereas mRNA levels of established PPARα-target genes were decreased (ranging from −45 to −82%) similar to what we reported in CM of ATGL-ko mice (16). FGF21 mRNA expression levels decreased (−51%) in mice with muscle-specific CGI-58 deficiency (CGI-58KOM) upon dietary administration of the PPARα agonist Wy14,643 (0.1%) whereas mRNA levels of established PPARα targets were normalized to WT levels (supplementary Fig. IA). It has been recently shown that cardiac-specific Perilipin5 overexpression (Plin5-Tg) provokes cardiac TG accumulation, which was compatible with normal heart function (20, 26). FGF21 mRNA levels were also increased (3.3-fold) in CM of Plin5-Tg mice (supplementary Fig. IB), although significantly less pronounced compared with ATGL-ko mice. In contrast to the induction of FGF21 expression in CM of mutant mice, mRNA expression of the FGF21 coreceptor β-Klotho, which is critically required for FGF21 signaling (7–9), was similarly low in CM of WT, ATGL-ko, and CGI-58KOM mice when compared with hepatic β-Klotho mRNA expression levels of WT mice (supplementary Fig. IC). In contrast to extremely low cardiac β-Klotho mRNA expression, Western blot analysis demonstrated distinct β-Klotho protein expression in CM, although the levels were unchanged in ATGL-ko and ATGL-koTgA mice compared with WT (supplementary Fig. ID).

ER stress has been linked to cardiac pathologies including oxygen and fuel starvation, cardiomyopathy, cardiac hypertrophy, and heart failure, among other heart disorders (27, 28). The marked defect in cardiac energy metabolism of ATGL-ko mice prompted us to examine protein expression levels of genes implicated in ER stress. Protein expression of the ER stress markers/chaperones BiP (glucose-regulated protein 78) and protein disulfide isomerase (Pdi) were exclusively increased in CM of ATGL-ko mice (Fig. 1B). In contrast, protein levels of Chop were barely detectable and comparable among all three genotypes (data not shown). The reconstitution of ATGL expression in CM of ATGL-ko mice (ATGL-koTgA) normalized protein levels to WT, suggesting that ER stress may induce Fgf21 mRNA expression in CM of ATGL-ko mice. Next we tested whether fasting per se affects mRNA expression levels of genes from the ER stress pathway. mRNA expression of genes from the ER stress pathway were unchanged or mildly decreased in overnight (ON)-fasted WT mice compared with fed mice, indicating that ON fasting does not induce an ER stress-related response (Fig. 1C).

A very recent study showed that ER stress strongly induces FGF21 mRNA expression in hepatoma cells and rat hepatocytes (29), and accordingly it is feasible that ER stress may be a trigger for FGF21 expression in CM of ATGL-ko mice (although it has been shown that ATGL-ko mice are protected from hepatic ER stress) (30). To address this hypothesis, we incubated H9C2 cardiomyotubes with 1.0 mM DTT for 4 h to induce cellular ER stress and quantitated mRNA levels of stress markers and FGF21. DTT treatment markedly induced FGF21 mRNA levels (20.2-fold) and increased mRNA expression of genes characteristic for the induction of stress signaling pathways (Fig. 1D), including Ddit3 (15.5-fold), a general stress marker, and increased mRNA levels of Grp78 (11.8-fold), ERdj4 (14.8-fold), and Xbp1 (4.5-fold), which are representative for induction of the unfolded protein response (31). To further examine whether ER stress is a potential inducer of FGF21 expression in cardiomyocytes, we incubated differentiated H9C2 cardiomyotubes with differentiation medium containing tunicamycin (10 μg/ml) or 200 μM palmitate for 24 h, which are known inducers of ER stress (32, 33). Incubation with tunicamycin (Fig. 1E) or palmitate (Fig. 1F)

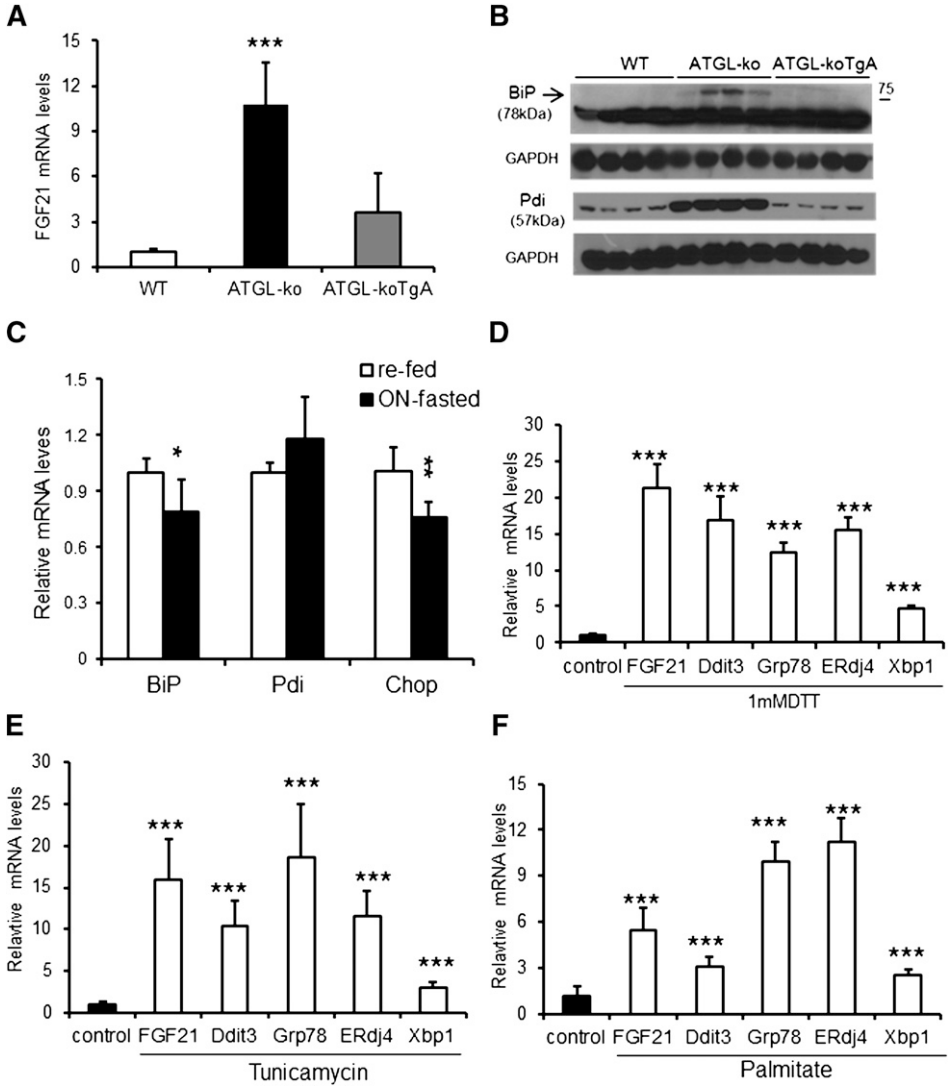

Fig. 1. Induced FGF21 mRNA expression in CM of ATGL-ko mice and in cardiac cells upon ER stress. A: Relative FGF21 mRNA expression levels in CM of fasted 14-week-old WT mice, ATGL-deficient mice (ATGL-ko), and ATGL-ko mice with cardiac-exclusive expression of an ATGL transgene (ATGL-koTgA) (n = 4–5). B: BiP (Grp78) and Pdi protein expression in CM lysates obtained from fasted WT, ATGL-ko, and ATGL-koTgA mice determined by Western blot analysis. GAPDH served as loading control. C: Relative mRNA levels of the ER stress markers BiP (Grp78), Pdi, and Chop in CM of 14-week-old re-fed WT compared with ON-fasted WT mice (n = 5–6). D: ER stress induced by DTT treatment of H9C2 cardiomyotubes provokes a substantial increase in FGF21 mRNA levels. ER stress signature of differentiated H9C2 cells upon DTT (1 mM) treatment was evidenced by the increase in mRNA expression of a general stress gene (Ddit3) and unfolded-protein response (UPR)-specific genes (Grp78, ERdj4 and Xbp1) compared with untreated cells. Tunicamycin (10 μg/ml) (E) or palmitate incubation (200 μM palmitate complexed with BSA) (F) of differentiated H9C2 cardiomyotubes similarly induced FGF21 mRNA expression paralleled by increased mRNA levels of ER stress characteristic genes. DMSO (0.5%) was used as solvent control for tunicamycin treatment. Data are mean + SD (n = 3). * $P < 0.05$, ** $P < 0.01$, and *** $P < 0.001$.

markedly triggers FGF21 mRNA expression, accompanied by increased mRNA levels of genes implicated in the ER stress pathway (ranging from 2.5- to 18.6-fold). Together, these data strongly suggest that ER stress is an inducer of FGF21 expression in cardiomyocytes.

Induction of cardiac FGF21 upon fasting and its impact on TG homeostasis in cardiomyotubes

Intrigued by our findings that FGF21 expression is induced in the myopathic heart, we asked whether FGF21 expression in the heart is also regulated by the body's energy status. Cardiac FGF21 mRNA expression levels are substantially increased in overnight fasted WT mice (4.9-fold), and levels remained high (4.1-fold increased) upon prolonged fasting for 24 h (**Fig. 2A**). In the fasted state, the heart relies more on TG as energy substrate. Fasting-induced FGF21 expression may indicate a potential role of FGF21 in cardiac TG metabolism. Therefore, we examined the impact of FGF21 overexpression on TG homeostasis in H9C2 rat cardiomyoblast cells. H9C2 cells were

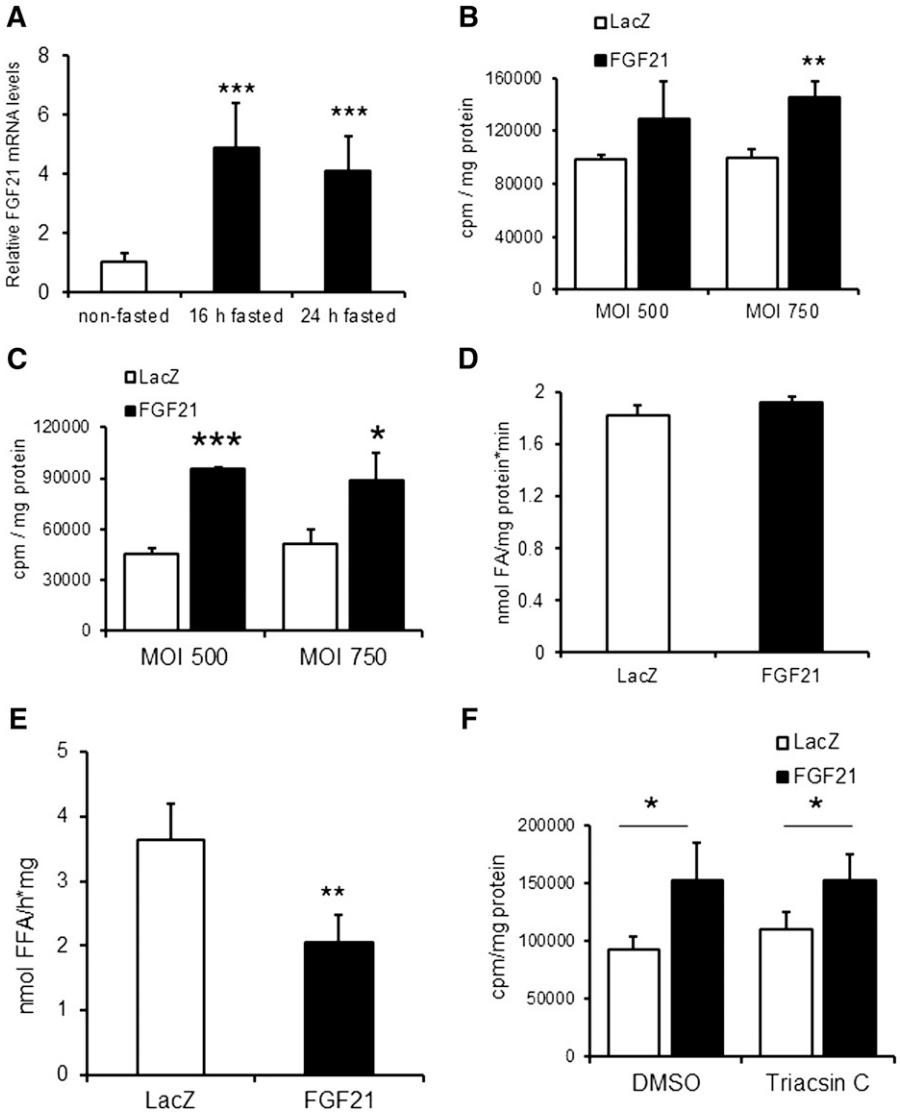

Fig. 2. FGF21 expression is induced in CM upon fasting and adenovirus-mediated FGF21 expression interferes with TG homeostasis in infected H9C2 cardiomyotubes. A: Cardiac FGF21 mRNA expression determined by quantitative RT-PCR in CM prepared from nonfasted 8-week-old male C57BL6 mice or from mice fasted for 16 and 24 h, respectively (n = 4–5). B: Measurement of FA incorporation into TG of H9C2 cardiomyotubes overexpressing murine FGF21. H9C2 cardiomyotubes (10 days of differentiation) were infected with LacZ or FGF21 encoding adenovirus at MOI 500 and 750, respectively. One day after infection, cells were incubated for 16 h with oleic acid containing [^{14}C]oleic acid as radioactive tracer. The incorporation of radioactivity into the TG moiety was determined by liquid scintillation counting of the TG fraction excised after TLC separation (n = 5). C: Measurement of [^{14}C]oleic acid incorporation into TG upon FGF21 overexpression as described above except for serum deprivation (4 h) before neutral lipid extraction (n = 5). D: FA uptake in differentiated cardiomyotubes infected with lacZ- and FGF21-expressing adenoviruses. Infected H9C2 cardiac cells were serum starved for 1 h and then incubated with [^{14}C]oleic acid for 1 min for determination of radioactivity in cell lysates (n = 3). E: TG-hydrolytic activities in cell lysates prepared from differentiated H9C2 cells upon infection with lacZ- or FGF21-expressing adenovirus (n = 4). F: Intracellular FA incorporation into TG of H9C2 cardiomyotubes upon Triacsin C-mediated inhibition of FA-re-esterification (n = 4). Data are mean + SD. * $P < 0.05$, ** $P < 0.01$, and *** $P < 0.001$.

differentiated to cardiomyotubes and infected with recombinant adenovirus expressing murine FGF21 or lacZ (as control) at 500 or 750 MOI. FGF21 protein was detectable in cell lysates after infection with FGF21-encoding adenovirus as well as in the medium after TCA precipitation, demonstrating that FGF21 is also secreted from differentiated H9C2 cells (supplementary Fig. II).

Two days after infection, cardiomyotubes were incubated overnight (16 h) with oleic acid containing ^{14}C-labeled oleic acid as radioactive tracer, and lipids were extracted and analyzed by TLC. Adenovirus-mediated FGF21 expression increased the incorporation of radioactivity into the cellular TG pool of H9C2 cardiomyoblasts (+31% and +46% at MOI 500 and 750, respectively)

compared with cells infected with lacZ control adenovirus (Fig. 2B). The increase in oleic acid incorporation into TG was even more pronounced under serum-starved conditions, ranging from +73% up to +111% (Fig. 2C). The increased incorporation of FA into TG of H9C2 cardiomyotubes upon infection with the FGF21 coding adenovirus can be the consequence of elevated FA uptake, impaired lipolysis, or preferential reesterification of released FAs after TG breakdown. To address this question, we first investigated cellular FA uptake of H9C2 cardiomyotubes upon short-term (1 min) incubation with ^{14}C-labeled oleic acid. FA uptake, calculated by the amount of intracellular radioactivity in cell lysates, was similar in FGF21-overexpressing cells compared with lacZ (Fig. 2D). We found that the TG hydrolytic activity in FGF21-expressing cells was markedly reduced (−44%) compared with control (lacZ) cells (Fig. 2E). These findings suggested that the increased TG deposition in H9C2 cells is a consequence of downregulated TG catabolism. FAs generated by intracellular TG catabolism can be re-esterified into the cellular TG pool in a futile cycle, which could additionally affect intracellular TG homeostasis. To examine the impact of FGF21 expression on FA re-esterification and TG homeostasis, H9C2 cardiomyotubes were again infected with respective adenoviruses and loaded overnight with radiolabeled oleic acid. On the next day, the medium was replaced by serum-free medium containing the acyl-CoA synthetase inhibitor Triacsin C to prevent re-esterification of liberated FAs. We found that the incorporation of radioactivity into the cellular TG pool was increased to a similar extent in cells infected with the FGF21-expressing adenovirus independent of the presence of Triacsin C (Fig. 2F) compared with control cells (lacZ), indicating that FA re-esterification was affected by FGF21 overexpression.

Increased glucose uptake and oxidation in cardiomyotubes expressing FGF21

Impaired TG catabolism in differentiated H9C2 cells overexpressing FGF21 may promote a metabolic switch to enhanced glucose oxidation. To examine whether FGF21 overexpression affects glucose uptake in H9C2 cells, differentiated H9C2 cells were infected with FGF21 and lacZ adenovirus. After 48 h, cardiomyotubes were serum starved and then incubated with or without insulin before the addition of 2-deoxy-D-glucose (2-DG). Infection with recombinant FGF21 adenovirus significantly increased 2-DG uptake (+32%) compared with lacZ controls (**Fig. 3A**). The incubation with insulin increased 2-DG glucose uptake in lacZ- and FGF21-expressing H9C2 cardiac cells to a similar extent (+39% and +38%, respectively), indicating that FGF21 expression affects glucose uptake in an insulin-independent manner. Furthermore, FGF21-expressing cardiomyotubes exhibited an elevated release of $^{14}CO_2$ (+67%) after incubation with ^{14}C-labeled glucose compared with lacZ controls, which is indicative of increased glucose oxidation in response to FGF21 overexpression (Fig. 3B). The respiratory defect of mitochondria prepared from ATGL-deficient mice prompted us to examine

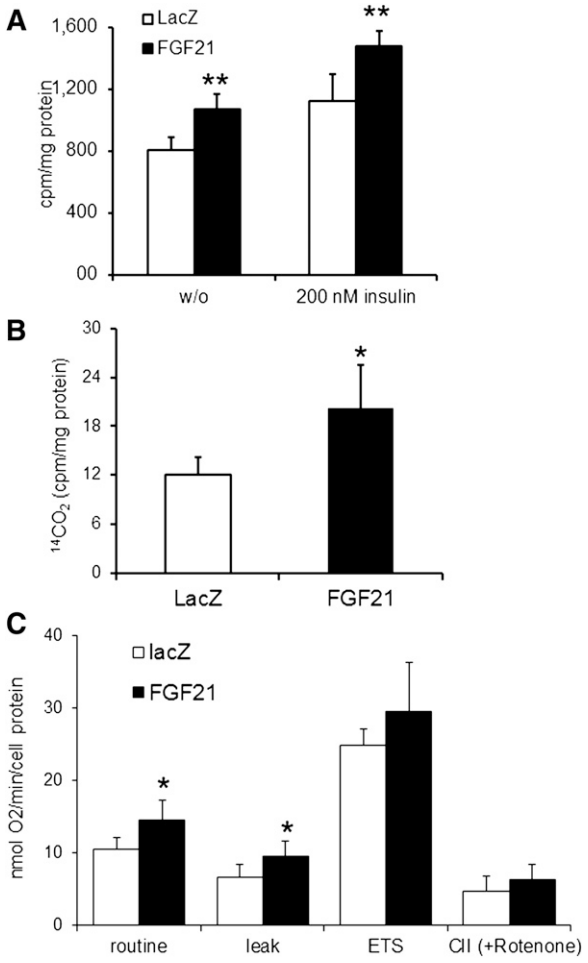

Fig. 3. Increased glucose uptake and oxidation in H9C2 cardiomyotubes infected with FGF21-expressing adenovirus. A: Glucose uptake of adenovirus-infected cardiomyotubes. H9C2 cardiomyotubes were infected with lacZ- or FGF21-expressing adenoviruses. Forty-eight hours after infection, cells were incubated with ^{3}H-labeled 2-deoxy-D-glucose for 5 min in the presence or absence of insulin ($n = 5$). The intracellular accumulation of ^{3}H-labeled 2-deoxy-D-glucose-6-phosphate was measured in cell lysates. The amount of $^{14}CO_2$ production (B) was determined as a measure of glucose oxidation after incubation with ^{14}C-labeled glucose for 2 h in lacZ- or FGF21-expressing H9C2 cardiomyotubes under serum-starved conditions (n = 4). C: Cellular respiration determined by high-resolution respirometry in differentiated cardiomyotubes upon infection with LacZ- and FGF21-encoding adenovirus (n = 6). Respiration was analyzed in intact cells using normal growth medium. Routine measurement encompasses all oxygen consuming processes in the cells. ADP-driven respiration was inhibited by oligomycin (LEAK), and the electron transfer system (ETS) was analyzed using the chemical uncoupler FCCP to determine maximal electron transfer. Data are mean + SD. * $P < 0.05$ and ** $P < 0.01$.

whether adenoviral-mediated FGF21 overexpression interferes with cellular respiration in differentiated H9C2 cardiomyotubes. Basal (routine) and oligomycin-inhibited oxygen flux (leak) in differentiated H9C2 cells infected with FGF21 adenovirus were 40% and 30% higher than in lacZ controls, respectively (Fig. 3C). Maximal electron transfer capacity and complex II-mediated respiration were unchanged between FGF21 and lacZ adenovirus-infected cells. Together, these data reveal that FGF21 overexpression

interferes with basal mitochondrial respiration and causes mild proton leak.

FGF21 is secreted from the heart of transgenic mice with cardiac-specific overexpression of FGF21

To extend our in vitro findings that ectopic FGF21 expression affects energy metabolism in H9C2 cardiomyotubes, we generated mice with cardiac-specific overexpression of murine FGF21 (CM-Fgf21). This mouse model was generated by cloning the murine Fgf21 cDNA downstream of the α-MHC promoter and microinjection of the transgene DNA construct (**Fig. 4A**) into the pronucleus of mouse embryos. Western blot analysis revealed highly increased FGF21-specific signals in CM lysates prepared from nonfasted CM-Fgf21 transgenic mice, whereas FGF21 protein signals were absent in cardiac tissue of controls (Fig. 4B). Plasma FGF21 levels (Fig. 4C) were markedly increased in CM-Fgf21 mice (11.4-fold) compared with WT mice, demonstrating that FGF21 is efficiently secreted from the heart of transgenic mice.

It has been reported that mice with hepatocyte-specific FGF21 overexpression showed markedly increased plasma FGF21 levels accompanied by growth retardation (4, 34). In our cardiac FGF21 transgenic mouse model, plasma FGF21 levels were also associated with decreased body weight (Fig. 4D), although to a very moderate extent (−19%). Moreover, CM-Fgf21 transgenic mice showed a moderate increase in body fat mass, which was paralleled by a reduction in lean body mass (Fig. 4E). Next, we measured plasma parameters of transgenic and WT mice, including ketone body and IGF-1 levels, which have been reported to be affected by increased circulating FGF21 levels (4, 34). Plasma glucose levels were mildly but significantly lowered in nonfasted and fasted CM-Fgf21 transgenic mice (−11.7 and −21.6%, respectively) compared with WT controls (**Table 1**). In contrast, plasma levels of nonesterified FAs and ketone bodies were significantly increased by 39.6% and 43.1% in fasted CM-Fgf21 transgenic mice compared with controls. Plasma IGF-1 levels were significantly lowered in plasma of nonfasted CM-Fgf21 mice, consistent with reported decreased IGF-1 levels of mice with hepatic FGF21 overexpression.

Increased cardiac TG levels and impaired TG catabolism and FAO in CM of FGF21 transgenic mice

Similar to the increase of endogenous TG levels upon FGF21 overexpression in H9C2 cardiomyotubes, cardiac-specific FGF21 overexpression provoked a 1.5-fold

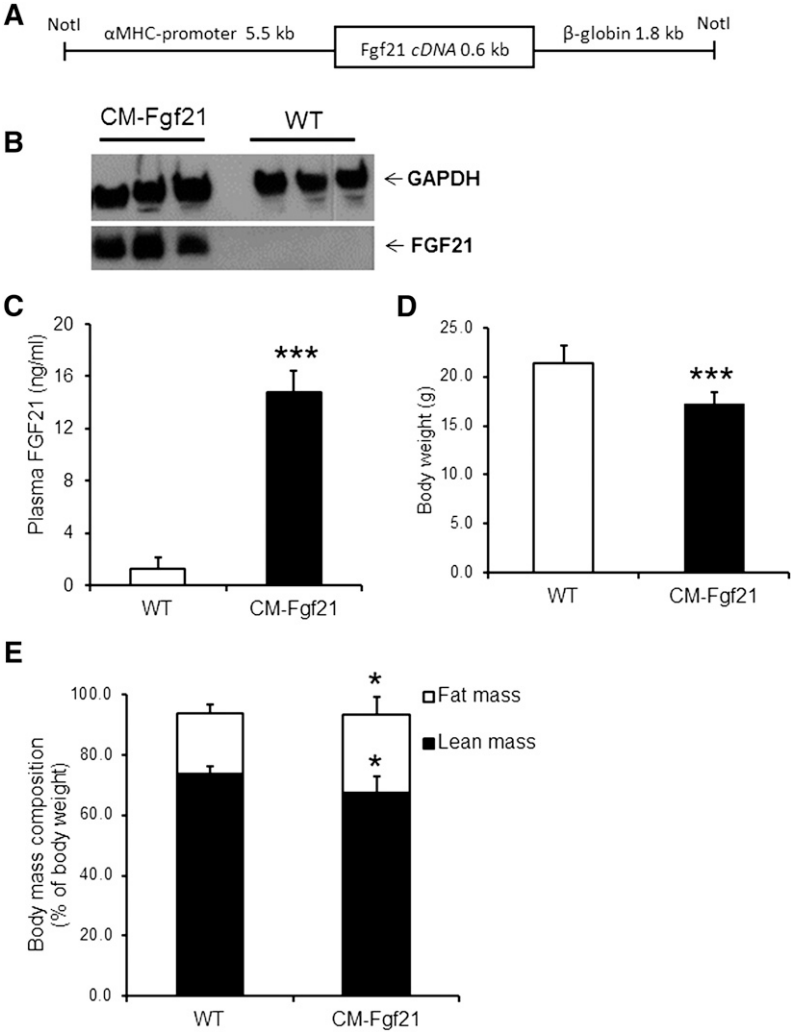

Fig. 4. Cardiac-specific FGF21 overexpression increases circulating FGF21 levels and affects body mass composition of FGF21 transgenic mice. A: Depiction of the FGF21 transgene used for microinjection and the generation of transgenic mice with cardiac-specific FGF21 overexpression. Mouse FGF21 cDNA was cloned downstream of the murine CM-specific α-myosin heavy chain (α-MHC) promoter. For mRNA stabilization, 1.8 kb of the nontranslated human β-globin gene were inserted at the 3′ end of the FGF21 cDNA. B: Western blot analysis of CM lysates (15 µg protein) incubated with a FGF21-specific antibody shows strong FGF21 expression in CM of FGF21 transgenic mice (CM-Fgf21) compared with WT. GAPDH served as loading control and cytosolic marker protein. C: Increased plasma FGF21 levels in 8-week-old FGF21 transgenic mice compared with WT controls (n = 4–6). FGF21 transgenic mice (16-week-old female mice) show a reduction in body weight (D) and lean body mass (E), whereas fat mass was increased (n = 6). Data are shown as mean + SD. * $P < 0.05$ and *** $P < 0.001$ versus WT.

TABLE 1. Plasma parameters determined in nonfasted and fasted CM-Fgf21 transgenic and WT mice

	Nonfasted		Fasted	
Parameter	WT	CM-Fgf21	WT	CM-Fgf21
Glucose (mg/dl)	170.5 ± 11.6	150.5 ± 12.6*	130.3 ± 24.7	102.2 ± 11.2*
TG (mg/dl)	140.1 ± 0.4	130.1 ± 0.3	76.6 ± 14.3	92.4 ± 10.0
NEFA (mmol/l)	0.78 ± 0.04	0.62 ± 0.10*	0.81 ± 0.14	1.13 ± 0.17**
β-Hb (mmol/l)	0.08 ± 0.02	0.15 ± 0.06*	0.51 ± 0.10	0.73 ± 0.09**
IGF-1 (ng/ml)	214.9 ± 53.1	93.1 ± 15.4**	n.d.	n.d.

Parameters were assayed with a glucometer, commercial kits, and an ELISA (IGF-1) in plasma samples obtained from nonfasted and overnight fasted 16- to 18-week-old female mice ($n \geq 5$). Data are mean + SD. β-Hb, β-hydroxybutyrate; IGF-1, insulin-like growth factor 1; NEFA, nonesterified FA.

* $P < 0.05$ versus WT mice.

** $P < 0.01$ versus WT mice.

increase in cardiac TG levels of CM-Fgf21 mice (**Fig. 5A**). Next we investigated whether overexpression of FGF21 cDNA affects mRNA levels of genes from the ER stress pathway. mRNA expression of the ER stress markers Grp78/BiP, Chop, Pdi, and Erdj4 were unchanged in CM-Fgf21 transgenics compared with controls (supplementary Fig. III). The increase in TG levels of CM-Fgf21 may be caused by changes in TG catabolism upon cardiac FGF21 overexpression. To address this hypothesis, we measured TG hydrolytic activities in CM lysates prepared from fasted mice when TGs are preferentially used as energy substrate. In agreement with our results from H9C2 cardiomyotubes, TG-hydrolytic activities were decreased (−34%) in CM preparations of CM-Fgf21 transgenics compared with WT (Fig. 5B).

The severe cardiac steatosis of ATGL-deficient mice was reported to be a consequence of impaired PPARα-activated expression of genes critically required for mitochondrial FAO (16). This finding prompted us to measure mRNA levels of established PPARα (and β/δ) target genes in CM of fasted transgenic mice (Fig. 5C). In contrast to ATGL-deficient mice, cardiac-specific FGF21 overexpression moderately affects mRNA expression of PPARα-regulated genes (Fig. 5C), including reduced mRNA levels of acyl-CoA oxidase (−27%), medium-chain acyl-CoA dehydrogenase (−17%), carnitine palmitoyltransferase 1b (−31%), and pyruvate dehydrogenase kinase 4 (–26%). Nonetheless, FAO, as assessed by $^{14}CO_2$ release from cardiac tissue lysates upon incubation with ^{14}C-labeled oleic acid, was significantly decreased (−41%) in CM preparations of CM-Fgf21 mice (Fig. 5D), whereas FAO was elevated (+59%) in liver lysates (Fig. 5E) from transgenic mice compared with WT. Decreased cardiac FAO in CM-Fgf21 transgenic mice suggests that cardiac overexpression of FGF21 may interfere with cardiac function. However, cardiac echography revealed normal heart function in CM-Fgf21 transgenic mice (supplementary Table I).

Moderate changes in glucose and whole body energy metabolism of CM-Fgf21 mice

Next we examined whether the observed changes in cardiac TG homeostasis of CM-Fgf21 mice affect cardiac glucose utilization. To measure tissue-specific glucose uptake, we injected glucose with [2-^{3}H]deoxyglucose as radioactive tracer and quantitated the formation of [2-^{3}H]deoxyglucose-6-phosphate ([2-^{3}H]2-DGP). [2-^{3}H]2-DGP formation as a measure of tissue glucose uptake and utilization was significantly increased in skeletal muscle of CM-Fgf21 transgenic (+51.9%) compared with WT controls, whereas CM and white adipose tissue showed a trend toward increased glucose uptake (**Fig. 6A**). However, phosphorylation (Thr172) of monophosphate-activated protein kinase (AMPK)α was similar in CM preparations of CM-Fgf21 mice compared with WT, implicating no significant changes in cardiac glucose utilization (supplementary Fig. IV). Glucose clearance (Fig. 6B) from the blood circulation of CM-Fgf21 mice was unchanged, implicating normal glucose tolerance in mice with cardiac-specific FGF21 overexpression. Finally, we monitored food intake, oxygen consumption, and carbon dioxide output for calculating RQ values as a measure for whole body energy metabolism. Food intake was significantly increased (+96%) in the light period of CM-Fgf21 mice (Fig. 6C) but was comparable to controls in the dark phase when food intake is generally increased. A RQ value of 1 would be theoretically reached when mice exclusively utilize glucose as energy fuel. The increase in the RQ value (+5.2%) of CM-Fgf21 mice (Fig. 6D) is an indication of a moderated change toward increased whole body glucose oxidation, which may be a consequence of the systemic increase in plasma FGF21 levels of transgenic mice. Taken together, these data indicate that the heart is able to secrete FGF21 into the circulation, leading to increased plasma FGF21 levels, which in turn affect cardiac and whole body energy metabolism.

DISCUSSION

For a long time, CM was not regarded as a FGF21 target tissue because of the extremely low or nondetectable expression of β-Klotho, which is a coreceptor required for FGF21 signaling (35–37). However, this view was changed by the very recent study of Planavila et al. (38) and Patel et al. (39) showing that both β-Klotho and FGF21 are expressed in cardiomyocytes and that mice globally lacking FGF21 exhibit increased heart weight and a cardiac proinflammatory signature.

Here we show that FGF21 mRNA expression is strongly increased in the steatotic heart of ATGL-ko mice. A recent

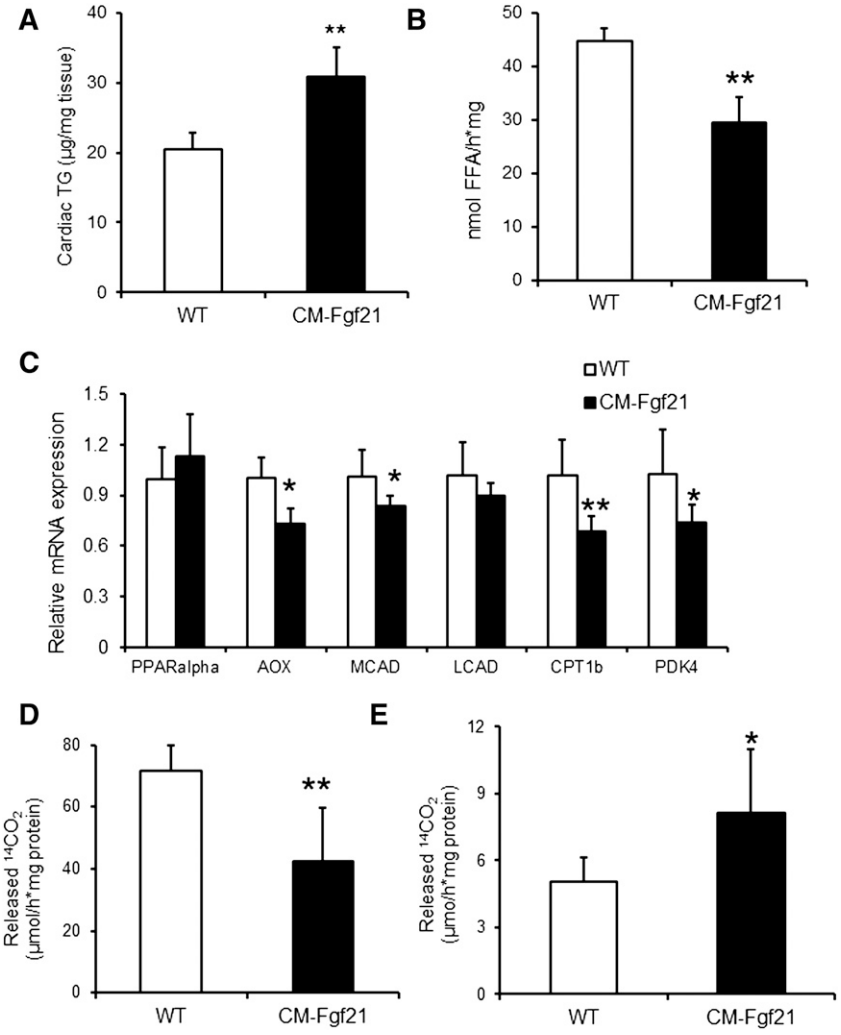

Fig. 5. Changes in cardiac TG homeostasis and FA catabolism in CM-Fgf21 transgenic mice. A: Increased TG levels in CM of 16-week-old fasted female mice upon cardiac-specific expression of the Fgf21 transgene (n = 4–5). B: TG hydrolytic activities in fat-poor homogenates (20,000 *g* infranatant) from cardiac tissue prepared from ON fasted mice (n = 4). C: mRNA expression levels of established PPARα (and β/δ) target genes determined by quantitative RT-PCR from RNA prepared from CM of 16-week-old, ON-fasted FGF21 transgenic and WT mice, respectively (n ⩾ 5). Release of ^{14}C-labeled CO_2 from mitochondrial preparations of cardiac (D) and hepatic (E) tissue of overnight fasted 3-month-old CM-Fgf21 and WT mice upon incubation with ^{14}C-labeled oleic acid (n = 4–5). Data are mean + SD. * $P < 0.05$ and ** $P < 0.01$ versus WT.

study shows that FGF21 mRNA expression is substantially reduced in the liver of ATGL-ko mice, which was paralleled by markedly reduced circulating FGF21 levels (19). The established role of FGF21 as PPARα-regulated gene in the liver (1, 3), together with the marked defect in PPARα-target gene expression in the liver of ATGL-ko mice (16) or in mice with hepatic ATGL knockdown (17), strongly suggests that the decline in hepatic FGF21 mRNA of these mouse models is primarily a PPARα defect. That PPARα-target gene expression is similarly impaired in CM of ATGL-ko mice indicates that the increase in cardiac FGF21 expression is a PPARα-independent defect. The marked reduction in cardiac FGF21 mRNA expression of ATGL-ko mice solely expressing an ATGL transgene in CM suggested that the induction of cardiac FGF21 expression originates from changes in cardiac metabolism and not from an adaptation to systemic changes in energy homeostasis of ATGL-ko mice. Energy starvation has been associated with cardiac ER stress (27). The increase in FGF21 mRNA expression in CM of ATGL-ko mice was associated with increased protein expression of genes from the ER stress pathway, and these changes were normalized to WT level when ATGL expression was exclusively reconstituted in the heart, suggesting that ER stress is a trigger for cardiac FGF21 expression. This assumption is further supported by the strong induction of FGF21 expression in differentiated H9C2 cardiomyotubes when treated with ER stress-activating agents including DTT, tunicamycin, and palmitate. Mice lacking the ATGL coactivator CGI-58 in CM (and skeletal muscle) (15) show a similar increase in cardiac FGF21 expression.

FGF21 mRNA levels dropped upon PPARα agonist administration, which has been shown to counteract cardiac

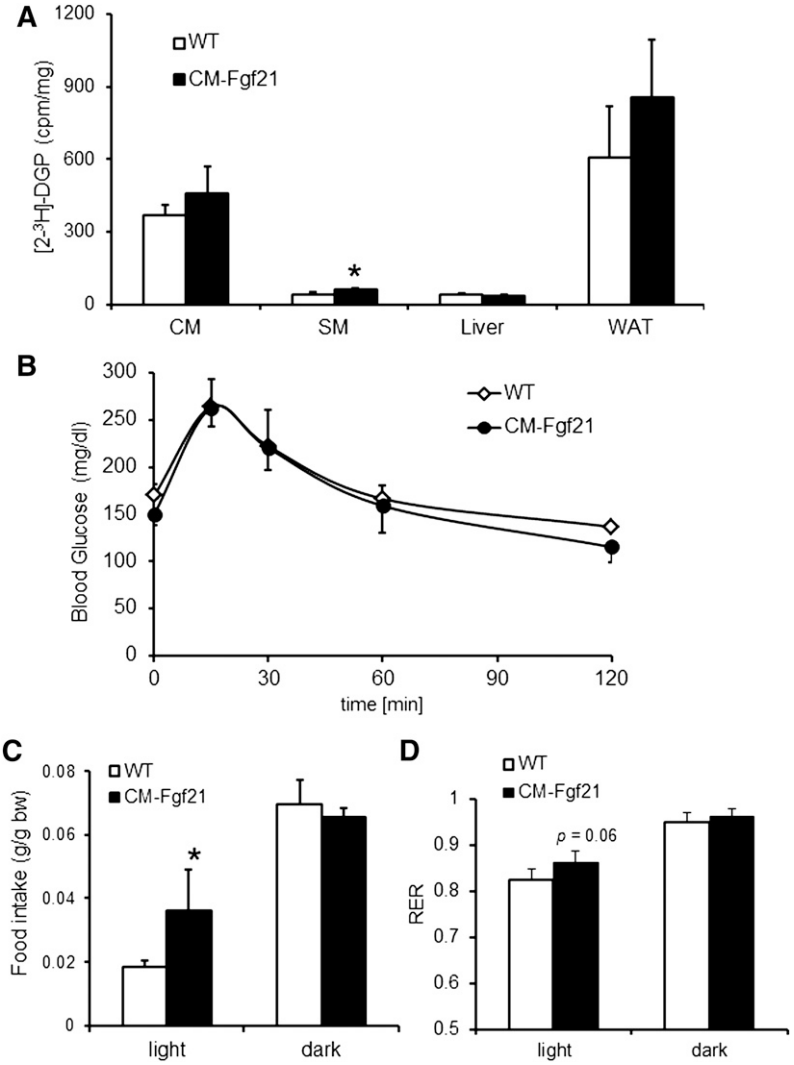

Fig. 6. Increased glucose uptake in skeletal muscle of FGF21 transgenic mice but normal glucose tolerance compared with WT. A: Tissue-specific glucose uptake determined in female transgenic mice fasted for 6 h. After injection of [2-^{3}H]deoxy-D-glucose as radioactive tracer, tissues were collected, and intracellular levels of [2-^{3}H]deoxy-D-glucose-6-phosphate were determined (n = 5). B: Glucose tolerance test performed in female mice fasted for 6 h (n = 5–6). Mean food intake (C) and RQ values (D) calculated from oxygen consumption and CO_2 production monitored over a period of 4 days in 16-week-old female mice (n = 4). Data are shown as mean + SD. * $P < 0.05$.

steatosis and to improve cardiac respiration in ATGL-deficient mice (16). It is conceivable that impaired mitochondrial respiration triggers ER stress in CM of ATGL-ko mice, which then induces FGF21 expression. In line with this assumption, the study by Dogan et al. (40) shows that an increase in the unfolded protein response in the heart (encompassing elevated Chop mRNA expression as in ATGL-ko hearts) linked to severe respiratory chain deficiency coincides with strongly elevated FGF21 expression. Finally, the moderate increase in cardiac FGF21 expression of Plin5 transgenic mice paralleled by mildly impaired mitochondrial respiration suggests that the extent in FGF21 expression correlates with the severity of mitochondrial dysfunction and possibly ER stress.

Recent findings further underline the potential role of FGF21 in the context of mitochondrial dysfunction. Studies have shown that skeletal muscle is an FGF21-producing tissue in mice (41) and humans (42) and that mitochondrial respiratory chain deficiency leads to an induction of FGF21 mRNA expression in skeletal muscle (43). There is strong evidence that increased FGF21 expression in skeletal muscle of the mutant mouse models and in humans (44) is causative for increased circulating FGF21 levels. These findings are in agreement with a diagnostic study in humans, where a strong correlation among muscle mitochondrial respiratory chain deficiencies and increased plasma FGF21 levels was described (45). The low FGF21 levels in ATGL-ko mice indicate reduced FGF21 levels as a diagnostic marker for hepatic steatosis, at least in mice.

In this study we also show that cardiac FGF21 mRNA expression increases in fasted WT mice (Fig. 2A), indicating a role of FGF21 in cardiac energy metabolism under nonpathological conditions. Adenovirus-mediated FGF21 overexpression significantly and consistently increased TG deposition in H9C2 cardiac cells, which was paralleled by reduced TG hydrolytic activity and increased glucose uptake. Furthermore, basal and oligomycin-sensitive respiration was moderately increased, further suggesting that FGF21 expression may affect mitochondrial function. However, the molecular origin behind mitochondrial proton leakage is unknown. The established role of FGF21 in stimulating glucose uptake (4, 46) can be extended to differentiated cardiomyotubes and is apparently linked to decreased TG utilization as energy fuel. To further assess the role of FGF21 in cardiac energy metabolism, we generated a mouse model with cardiac-specific overexpression

of murine FGF21. FGF21 was efficiently expressed and secreted from the heart of transgenic mice, leading to a similar phenotype compared with mice with hepatocyte-specific FGF21 overexpression (4, 34) encompassing increased plasma FGF21 levels, reduced body weight and lean body mass, increased plasma ketone body concentrations, and reduced blood glucose and plasma IGF-1 levels.

Consistent with changes in TG homeostasis upon FGF21 overexpression in H9C2 cardiomyotubes, we found increased TG deposition in CM of mice with cardiac-specific FGF21 overexpression, which was paralleled by decreased cardiac TG hydrolytic activities and a reduction in mitochondrial FAO. Furthermore, the expression of PPARα (and β/δ) target genes involved in mitochondrial FAO was moderately but significantly reduced, which could be a consequence of impaired lipolysis, as has been reported for mice lacking ATGL or CGI-58 specifically in muscle (15, 16). The observation that CM-Fgf21 mice exhibit normal heart function suggests that in these animals mitochondrial FAO is more moderately affected as compared with the marked defect in mitochondrial FAO and cardiac function of ATGL-deficient mice. CM-Fgf21 mice showed no significant changes in cardiac glucose uptake despite impaired TG catabolism. It is conceivable that cardiac glucose uptake in CM-Fgf21 is very mildly but constantly increased yet not significantly changed in our experimental approach. Although speculative, the increase in plasma ketone body levels of CM-Fgf21 transgenic mice may enhance cardiac ketone body utilization at the expense of TG, thereby sparing TG catabolism.

Recent studies showed that global FGF21 deficiency promotes cardiac hypertrophy (and proinflammatory pathways) and adversely affects heart function in response to ischemia (38, 47), which strongly suggests that the heart is a FGF21-responsive tissue. Furthermore, these studies demonstrate that β-Klotho may be expressed in low but sufficient levels in CM and thus allows FGF21 signaling via binding to β-Klotho in concert with fibroblast growth factor receptor 1. In line with these observations, we detected β-Klotho protein expression in CM of WT and ATGL-mutant mice, indicating that FGF21 might affect cardiac energy metabolism in an autocrine manner; this finding requires further investigation. Patel and colleagues showed that recombinant FGF21 administration improves cardiac function in hearts from obese rats (39), which might be also mediated via β-Klotho interaction. Taken together, results from our CM-Ffg21 mice indicate that cardiac FGF21 does not play a major role in cardiac energy metabolism under healthy conditions but may exert an important protective role in the diseased heart or act as a marker for cardiac dysfunction involving cardiac ER stress.

The authors thank Steven Kliewer for providing the FGF21 encoding adenoviral DNA and B. Juritsch, B. Seisser, and A. Steiner for their excellent technical assistance in mouse genotyping and housing.

REFERENCES

1. Badman, M. K., P. Pissios, A. R. Kennedy, G. Koukos, J. S. Flier, and E. Maratos-Flier. 2007. Hepatic fibroblast growth factor 21 is regulated by PPARalpha and is a key mediator of hepatic lipid metabolism in ketotic states. *Cell Metab.* **5:** 426–437.
2. Gälman, C., T. Lundåsen, A. Kharitonenkov, H. A. Bina, M. Eriksson, I. Hafström, M. Dahlin, P. Amark, B. Angelin, and M. Rudling. 2008. The circulating metabolic regulator FGF21 is induced by prolonged fasting and PPARalpha activation in man. *Cell Metab.* **8:** 169–174.
3. Inagaki, T., P. Dutchak, G. Zhao, X. Ding, L. Gautron, V. Parameswara, Y. Li, R. Goetz, M. Mohammadi, V. Esser, et al. 2007. Endocrine regulation of the fasting response by PPARalpha-mediated induction of fibroblast growth factor 21. *Cell Metab.* **5:** 415–425.
4. Kharitonenkov, A., T. L. Shiyanova, A. Koester, A. M. Ford, R. Micanovic, E. J. Galbreath, G. E. Sandusky, L. J. Hammond, J. S. Moyers, R. A. Owens, et al. 2005. FGF-21 as a novel metabolic regulator. *J. Clin. Invest.* **115:** 1627–1635.
5. Kharitonenkov, A., and P. Larsen. 2011. FGF21 reloaded: challenges of a rapidly growing field. *Trends Endocrinol. Metab.* **22:** 81–86.
6. Potthoff, M. J., S. A. Kliewer, and D. J. Mangelsdorf. 2012. Endocrine fibroblast growth factors 15/19 and 21: from feast to famine. *Genes Dev.* **26:** 312–324.
7. Kharitonenkov, A., J. D. Dunbar, H. A. Bina, S. Bright, J. S. Moyers, C. Zhang, L. Ding, R. Micanovic, S. F. Mehrbod, M. D. Knierman, et al. 2008. FGF-21/FGF-21 receptor interaction and activation is determined by betaKlotho. *J. Cell. Physiol.* **215:** 1–7.
8. Ogawa, Y., H. Kurosu, M. Yamamoto, A. Nandi, K. P. Rosenblatt, R. Goetz, A. V. Eliseenkova, M. Mohammadi, and M. Kuro-o. 2007. BetaKlotho is required for metabolic activity of fibroblast growth factor 21. *Proc. Natl. Acad. Sci. USA.* **104:** 7432–7437.
9. Suzuki, M., Y. Uehara, K. Motomura-Matsuzaka, J. Oki, Y. Koyama, M. Kimura, M. Asada, A. Komi-Kuramochi, S. Oka, and T. Imamura. 2008. betaKlotho is required for fibroblast growth factor (FGF) 21 signaling through FGF receptor (FGFR) 1c and FGFR3c. *Mol. Endocrinol.* **22:** 1006–1014.
10. Lefebvre, P., G. Chinetti, J. Fruchart, and B. Staels. 2006. Review series: Sorting out the roles of PPARα in energy metabolism and vascular homeostasis. *J. Clin. Invest.* **116:** 571–580.
11. Zechner, R., R. Zimmermann, T. O. Eichmann, S. D. Kohlwein, G. Haemmerle, A. Lass, and F. Madeo. 2012. FAT SIGNALS–lipases and lipolysis in lipid metabolism and signaling. *Cell Metab.* **15:** 279–291.
12. Haemmerle, G., A. Lass, R. Zimmermann, G. Gorkiewicz, C. Meyer, J. Rozman, G. Heldmaier, R. Maier, C. Theussl, S. Eder, et al. 2006. Defective lipolysis and altered energy metabolism in mice lacking adipose triglyceride lipase. *Science.* **312:** 734–737.
13. Zimmermann, R., J. G. Strauss, G. Haemmerle, G. Schoiswohl, R. Birner-Gruenberger, M. Riederer, A. Lass, G. Neuberger, F. Eisenhaber, A. Hermetter, and R. Zechner. 2004. Fat mobilization in adipose tissue is promoted by adipose triglyceride lipase. *Science.* 306: 1383–1386.
14. Lass, A., R. Zimmermann, G. Haemmerle, M. Riederer, G. Schoiswohl, M. Schweiger, P. Kienesberger, J. G. Strauss, G. Gorkiewicz, and R. Zechner. 2006. Adipose triglyceride lipase-mediated lipolysis of cellular fat stores is activated by CGI-58 and defective in Chanarin-Dorfman Syndrome. *Cell Metab.* **3:** 309–319.
15. Zierler, K. A., D. Jaeger, N. M. Pollak, S. Eder, G. N. Rechberger, F. P. W. Radner, G. Woelkart, D. Kolb, A. Schmidt, M. Kumari, et al. 2013. Functional cardiac lipolysis in mice critically depends on comparative gene identification-58. *J. Biol. Chem.* **288:** 9892–9904.
16. Haemmerle, G., T. Moustafa, G. Woelkart, S. Büttner, A. Schmidt, T. van de Weijer, M. Hesselink, D. Jaeger, P. C. Kienesberger, K. Zierler, et al. 2011. ATGL-mediated fat catabolism regulates cardiac mitochondrial function via PPAR-α and PGC-1. *Nat. Med.* **17:** 1076–1085.
17. Ong, K. T., M. T. Mashek, S. Y. Bu, A. S. Greenberg, and D. G. Mashek. 2011. Adipose triglyceride lipase is a major hepatic lipase that regulates triacylglycerol turnover and fatty acid signaling and partitioning. *Hepatology.* **53:** 116–126.
18. Sapiro, J. M., M. T. Mashek, A. S. Greenberg, and D. G. Mashek. 2009. Hepatic triacylglycerol hydrolysis regulates peroxisome proliferator-activated receptor alpha activity. *J. Lipid Res.* **50:** 1621–1629.

19. Jha, P., T. Claudel, A. Baghdasaryan, M. Mueller, E. Halilbasic, S. K. Das, A. Lass, R. Zimmermann, R. Zechner, G. Hoefler, and M. Trauner. 2014. Role of adipose triglyceride lipase (PNPLA2) in protection from hepatic inflammation in mouse models of steatohepatitis and endotoxemia. *Hepatology.*
20. Pollak, N. M., M. Schweiger, D. Jaeger, D. Kolb, M. Kumari, R. Schreiber, S. Kolleritsch, P. Markolin, G. F. Grabner, C. Heier, et al. 2013. Cardiac-specific overexpression of perilipin 5 provokes severe cardiac steatosis via the formation of a lipolytic barrier. *J. Lipid Res.* **54:** 1092–1102.
21. Subramaniam, A., J. Gulick, J. Neumann, S. Knotts, and J. Robbins. 1993. Transgenic analysis of the thyroid-responsive elements in the alpha-cardiac myosin heavy chain gene promoter. *J. Biol. Chem.* **268:** 4331–4336.
22. Teng, B., S. Blumenthal, T. Forte, N. Navaratnam, J. Scott, A. M. Gotto, and L. Chan. 1994. Adenovirus-mediated gene transfer of rat apolipoprotein B mRNA-editing protein in mice virtually eliminates apolipoprotein B-100 and normal low density lipoprotein production. *J. Biol. Chem.* **269:** 29395–29404.
23. Folch, J., M. Lees, and G. H. Sloane Stanley. 1957. A simple method for the isolation and purification of total lipides from animal tissues. *J. Biol. Chem.* **226:** 497–509.
24. Hirschey, M. D., T. Shimazu, E. Goetzman, E. Jing, B. Schwer, D. B. Lombard, C. A. Grueter, C. Harris, S. Biddinger, O. R. Ilkayeva, et al. 2010. SIRT3 regulates mitochondrial fatty-acid oxidation by reversible enzyme deacetylation. *Nature.* **464:** 121–125.
25. Song, Q., A. G. Schmidt, H. S. Hahn, A. N. Carr, B. Frank, L. Pater, M. Gerst, K. Young, B. D. Hoit, B. K. McConnell, et al. 2003. Rescue of cardiomyocyte dysfunction by phospholamban ablation does not prevent ventricular failure in genetic hypertrophy. *J. Clin. Invest.* **111:** 859–867.
26. Wang, H., U. Sreenivasan, D-W. Gong, K. A. O'Connell, E. R. Dabkowski, P. A. Hecker, N. Ionica, M. Konig, A. Mahurkar, Y. Sun, et al. 2013. Cardiomyocyte-specific perilipin 5 overexpression leads to myocardial steatosis and modest cardiac dysfunction. *J. Lipid Res.* **54:** 953–965.
27. Groenendyk, J., L. B. Agellon, and M. Michalak. 2013. Coping with endoplasmic reticulum stress in the cardiovascular system. *Annu. Rev. Physiol.* **75:** 49–67.
28. Minamino, T., and M. Kitakaze. 2010. ER stress in cardiovascular disease. *J. Mol. Cell. Cardiol.* **48:** 1105–1110.
29. Schaap, F. G., A. E. Kremer, W. H. Lamers, P. L. M. Jansen, and I. C. Gaemers. 2013. Fibroblast growth factor 21 is induced by endoplasmic reticulum stress. *Biochimie.* **95:** 692–699.
30. Fuchs, C. D., T. Claudel, P. Kumari, G. Haemmerle, M. J. Pollheimer, T. Stojakovic, H. Scharnagl, E. Halilbasic, J. Gumhold, D. Silbert, et al. 2012. Absence of adipose triglyceride lipase protects from hepatic endoplasmic reticulum stress in mice. *Hepatology.* **56:** 270–280.
31. Malhi, H., and R. J. Kaufman. 2011. Endoplasmic reticulum stress in liver disease. *J. Hepatol.* **54:** 795–809.
32. Wei, Y., D. Wang, F. Topczewski, and M. J. Pagliassotti. 2006. Saturated fatty acids induce endoplasmic reticulum stress and apoptosis independently of ceramide in liver cells. *Am. J. Physiol. Endocrinol. Metab.* **291:** E275–E281.
33. Zhang, P. L., M. Lun, J. Teng, J. Huang, T. M. Blasick, L. Yin, G. A. Herrera, and J. Y. Cheung. 2004. Preinduced molecular chaperones in the endoplasmic reticulum protect cardiomyocytes from lethal injury. *Ann. Clin. Lab. Sci.* **34:** 449–457.
34. Inagaki, T., V. Y. Lin, R. Goetz, M. Mohammadi, D. J. Mangelsdorf, and S. A. Kliewer. 2008. Inhibition of growth hormone signaling by the fasting-induced hormone FGF21. *Cell Metab.* **8:** 77–83.
35. Xu, J., S. Stanislaus, N. Chinookoswong, Y. Y. Lau, T. Hager, J. Patel, H. Ge, J. Weiszmann, S-C. Lu, M. Graham, et al. 2009. Acute glucose-lowering and insulin-sensitizing action of FGF21 in insulin-resistant mouse models–association with liver and adipose tissue effects. *Am. J. Physiol. Endocrinol. Metab.* **297:** E1105–E1114.
36. Fisher, F. M., J. L. Estall, A. C. Adams, P. J. Antonellis, H. A. Bina, J. S. Flier, A. Kharitonenkov, B. M. Spiegelman, and E. Maratos-Flier. 2011. Integrated regulation of hepatic metabolism by fibroblast growth factor 21 (FGF21) in vivo. *Endocrinology.* **152:** 2996–3004.
37. Berglund, E. D., C. Y. Li, H. A. Bina, S. E. Lynes, M. D. Michael, A. B. Shanafelt, A. Kharitonenkov, and D. H. Wasserman. 2009. Fibroblast growth factor 21 controls glycemia via regulation of hepatic glucose flux and insulin sensitivity. *Endocrinology.* **150:** 4084–4093.
38. Planavila, A., I. Redondo, E. Hondares, M. Vinciguerra, C. Munts, R. Iglesias, L. A. Gabrielli, M. Sitges, M. Giralt, M. van Bilsen, et al. 2013. Fibroblast growth factor 21 protects against cardiac hypertrophy in mice. *Nat. Commun.* **4:** 2019.
39. Patel, V., R. Adya, J. Chen, M. Ramanjaneya, M. F. Bari, S. K. Bhudia, E. W. Hillhouse, B. K. Tan, and H. S. Randeva. 2014. Novel insights into the cardio-protective effects of FGF21 in lean and obese rat hearts. *PLoS ONE.* **9:** e87102.
40. Dogan, S. A., C. Pujol, P. Maiti, A. Kukat, S. Wang, S. Hermans, K. Senft, R. Wibom, E. I. Rugarli, and A. Trifunovic. 2014. Tissue-specific loss of DARS2 activates stress responses independently of respiratory chain deficiency in the heart. *Cell Metab.* **19:** 458–469.
41. Izumiya, Y., H. A. Bina, N. Ouchi, Y. Akasaki, A. Kharitonenkov, and K. Walsh. 2008. FGF21 is an Akt-regulated myokine. *FEBS Lett.* **582:** 3805–3810.
42. Hojman, P., M. Pedersen, A. R. Nielsen, R. Krogh-Madsen, C. Yfanti, T. Akerstrom, S. Nielsen, and B. K. Pedersen. 2009. Fibroblast growth factor-21 is induced in human skeletal muscles by hyperinsulinemia. *Diabetes.* **58:** 2797–2801.
43. Tyynismaa, H., C. J. Carroll, N. Raimundo, S. Ahola-Erkkilä, T. Wenz, H. Ruhanen, K. Guse, A. Hemminki, K. E. Peltola-Mjøsund, V. Tulkki, et al. 2010. Mitochondrial myopathy induces a starvation-like response. *Hum. Mol. Genet.* **19:** 3948–3958.
44. Crooks, D. R., T. G. Natarajan, S. Y. Jeong, C. Chen, S. Y. Park, H. Huang, M. C. Ghosh, W.-H. Tong, R. G. Haller, C. Wu, and T. A. Rouault. 2014. Elevated FGF21 secretion, PGC-1α and ketogenic enzyme expression are hallmarks of iron-sulfur cluster depletion in human skeletal muscle. *Hum. Mol. Genet.*
45. Suomalainen, A., J. M. Elo, K. H. Pietiläinen, A. H. Hakonen, K. Sevastianova, M. Korpela, P. Isohanni, S. K. Marjavaara, T. Tyni, S. Kiuru-Enari, et al. 2011. FGF-21 as a biomarker for muscle-manifesting mitochondrial respiratory chain deficiencies: a diagnostic study. *Lancet Neurol.* **10:** 806–818.
46. Dostálová, I., D. Haluzíková, and M. Haluzík. 2009. Fibroblast growth factor 21: a novel metabolic regulator with potential therapeutic properties in obesity/type 2 diabetes mellitus. *Physiol. Res.* **58:** 1–7.
47. Liu, S. Q., D. Roberts, A. Kharitonenkov, B. Zhang, S. M. Hanson, Y. C. Li, L-Q. Zhang, and Y. H. Wu. 2013. Endocrine protection of ischemic myocardium by FGF21 from the liver and adipose tissue. *Sci. Rep.* **3:** 2767.